Estuarine, Coastal and Shelf Science 143 (2014) 20–31

Contents lists available at ScienceDirect

Estuarine, Coastal and Shelf Science

journal homepage: www.elsevier.com/locate/ecss

Swash zone moisture dynamics and unsaturated infiltration in two sandy beach aquifers

James W. Heiss [a], William J. Ullman [b], Holly A. Michael [a,c,*]

[a] Department of Geological Sciences, University of Delaware, Newark, DE 19716, USA
[b] School of Marine Science and Policy, University of Delaware, Lewes, DE 19958, USA
[c] Department of Civil and Environmental Engineering, University of Delaware, Newark, DE 19716, USA

ARTICLE INFO

Article history:
Received 11 June 2013
Accepted 13 March 2014
Available online 22 March 2014

Keywords:
beach groundwater circulation
wave swash
intertidal zone
water table fluctuations
coastal aquifer
submarine groundwater discharge

ABSTRACT

The intertidal zone of coastal aquifers is a dynamic region of mixing between saline surface water and fresh groundwater. Groundwater circulation in this zone is affected by complex forcing mechanisms that operate on a range of timescales and can regulate chemical fluxes to marine environments. We evaluated wave swash-induced infiltration and associated flow dynamics in the unsaturated region of two sandy beach aquifers with differing wave conditions and beach morphologies. Moisture and pressure sensors were used to measure fluctuations in water content, water table elevation, and hydraulic gradients at high frequencies (5 Hz) in the swash zone at mean lower low water, mean sea level, and mean higher high water. Water content in the unsaturated region of the swash zone responded to wave overtopping and swash infiltration, with a rapid rise in water content followed by a slower decline. Swash-induced unsaturated infiltration rates, calculated from water content response, were lowest near low tide and increased up the beachface with inflow highest near high tide at both sites, consistent with an increase in water table depth up the beach. Unsaturated infiltration was 1.6 m^3/m per tidal cycle at the wave-dominated beach and 0.4 m^3/m per tidal cycle at the tide-dominated beach. Saturated pore pressure measurements show that a water table mound formed as a consequence of swash infiltration that migrated up the beach during rising tide, leading to divergent seaward/landward groundwater flow. The results demonstrate the significant and spatially variable effects of wave swash on moisture dynamics in the unsaturated zone of beach aquifers, and show that these effects depend on wave conditions and beach characteristics. Results have implications for understanding transport and reaction of solutes in this biogeochemically active zone.

1. Introduction

The intertidal zone of beach aquifers is a dynamic area of mixing between terrestrially-derived fresh and marine-derived saline waters. In this zone, the inland hydraulic gradient drives freshwater discharge to the sea, and tides and waves drive seawater into the aquifer through a combination of saturated and unsaturated flow. The resulting mixing zone is bounded by the high tide level or the extent of swash run-up and a lower Ghyben–Herzberg interface (Boufadel, 2000; Turner and Acworth, 2004; Robinson et al., 2006). The infiltration of seawater by waves and tides alters the salinity distribution in the beach aquifer, the directions and rates of groundwater flow, and the rates of submarine groundwater discharge (SGD) (Michael et al., 2005; Vandenbohede and Lebbe, 2005; Robinson et al., 2007; Li et al., 2008). As a result of this infiltration, seawater circulating through beach aquifers can comprise a significant portion of SGD (Gallagher et al., 1996; Robinson et al., 1998; Boehm et al., 2006; Sieyes et al., 2008). Furthermore, mixing between through-flowing freshwater and circulating saltwater in the beach aquifer has been shown to impact biogeochemical processes that affect the transport of land-derived solutes to the sea (Charette and Sholkovitz, 2002; Kroeger and Charette, 2008; Santos et al., 2008; Spiteri et al., 2008; Loveless and Oldham, 2009; Santoro, 2009). Infiltration processes occurring in the swash zone, the area between the wave breaking point and the location of maximum wave run-up, can affect the biogeochemical conditions of the beach aquifer by introducing dissolved oxygen and reactive organic matter to intertidal sediments (e.g.

* Corresponding author. Department of Geological Sciences, University of Delaware, Newark, DE 19716, USA.
E-mail addresses: jheiss@udel.edu (J.W. Heiss), ullman@udel.edu (W.J. Ullman), hmichael@udel.edu (H.A. Michael).

http://dx.doi.org/10.1016/j.ecss.2014.03.015
0272-7714/

McLachlan et al., 1985; Ullman et al., 2003; Orr et al., 2005; Charbonnier et al., 2013), and by controlling chemical residence times (Boufadel et al., 2007; Bakhtyar et al., 2013). Swash–groundwater interactions are also important for sediment transport and beach morphology (e.g. Hegge and Masselink, 1991; Turner and Nielsen, 1997; Baldock et al., 2001; Butt et al., 2001; Cartwright et al., 2006).

Few studies have focused on flow within the unsaturated zone of the beach and the impact of unsaturated flow on the water circulation patterns within the beach aquifer. Pollock and Hummon (1971) developed a classification scheme for the beach subsurface based on the water content and water content variability. Turner (1993a) monitored water content above and below the water table on two morphologically contrasting sandy beaches to construct a conceptual model of moisture dynamics within the beach landward of the intertidal zone. These measurements showed that water content between the dune line and the high tide mark was temporally and spatially variable over a tidal cycle.

A number of field studies investigating pore pressure response to wave run-up suggest that moisture conditions in the unsaturated region of the swash zone are important to intertidal flow processes. Pore pressure measurements taken within and above the capillary fringe indicate that pressure responses are caused by filling and draining of the beach sediments with each swash cycle (Horn et al., 1998; Baldock et al., 2001; Cartwright et al., 2006). The magnitude and rate of the pressure response can be explained by the presence of the capillary fringe above the water table, its proximity to the land surface, and the distance from the seepage face (Cartwright et al., 2006). However, direct observations of moisture content dynamics related to the vertical movement of infiltrating seawater through the unsaturated zone to the water table caused by wave swash have not been made.

Estimates of swash infiltration into the unsaturated zone have been made in the laboratory and the field. Steenhauer et al. (2011) conducted laboratory experiments in which a wetting front (the boundary between the saturated zone of infiltrating water and the unsaturated zone at depth) was monitored through the glass wall of a flume using digital photography. Masselink and Turner (2012) estimated swash infiltration in the laboratory by comparing run-up and run-down discharge. Others (e.g. McLachlan, 1979; McLachlan et al., 1985) calculated potential maximum swash inflow volumes as the pore volume of an initially unsaturated wedge extending horizontally from the groundwater discharge point near the base of the beach to the run-up limit high on the beach, and vertically from the beach surface to the water table. Infiltration volumes have also been determined from changes in water table elevations in wells (e.g., Kang et al., 1994). The above methods provide integrated infiltration volumes, but it is unclear how infiltration varies over a broad range of spatial scales (at a single location, across the swash zone, across the intertidal zone, and across different beaches). Additionally, cumulative swash infiltration across the unsaturated beachface over a tidal cycle has not been quantified.

A number of recent investigations have examined the time-averaged response of the water table to swash input through the unsaturated zone (Austin and Masselink, 2006; Masselink and Turner, 2012; Turner and Masselink, 2012). These studies, all performed on gravel beaches, demonstrate that swash infiltration results in a rise in the mean water table directly beneath the active swash zone. This forms a water table mound, parallel to the shore, leading to horizontal flow in the seaward direction across the lower beachface and landward flow landward of the mound. Laboratory measurements of water table elevations spanning the length of the mound have been conducted on the time scale of wave swash (e.g. Boufadel et al., 2011; Steenhauer et al., 2011). Horizontal hydraulic gradients within the mound are likely to vary with each swash event as the water table rises and falls during run-up and run-down. Thus, instantaneous horizontal flow rates may differ from those calculated using time-averaged hydraulic gradients and may lead to enhanced mixing as a result of rapidly changing flow directions. However, these gradients have not been measured at swash frequencies.

We build on previous work by quantifying the rates of seawater infiltration into the unsaturated beachface and the resulting moisture dynamics in the beach aquifer at contrasting wave- and tide-dominated beaches. The primary objectives of this work are to: 1) explore the influence of wave swash on water content within the swash zone; 2) determine the spatial variability of swash infiltration rates and volumes within the unsaturated region of the swash zone and between two beaches with differing intertidal zone widths; 3) understand the response of horizontal hydraulic gradients beneath the swash zone due to wave swash and tides.

2. Background: beach groundwater–surface water interactions

The primary mechanisms that induce saltwater recharge and circulation in the intertidal zone of the beach aquifer are waves and tides (Fig. 1a). Wave forcing leads to setup, an upward tilt in mean sea level that increases onshore in the surf zone and contributes to a persistent water table over-height in the saturated zone (Longuet-Higgins, 1983). Assuming a constant shoreline position, the mean on-shore hydraulic gradient that results from wave set-up drives steady localized saturated saltwater infiltration and circulation, D_w, between the water table-beachface intersection (i.e. exit point; Turner, 1993b) and the base of the beach (Li et al., 1999; process 1 in Fig. 1a). Along this saturated beachface, seawater infiltration and exfiltration can also occur at the frequency of individual swash events (D_{ss}; process 2 in Fig. 1a). Numerous studies have quantified vertical flow rates across this region of the beach to better understand sediment transport dynamics in the swash zone (e.g. Turner and Masselink, 1998; Butt et al., 2001). The third and less well understood pathway by which waves can drive water into the beach aquifer is across the unsaturated part of the beach. Swash infiltration along this pathway only occurs when the swash lens extends landward of the exit point; therefore only the largest amplitude swash events are able to drive this process (Austin and Masselink, 2006) (D_{su}; process 3 in Fig. 1a). Although few swash events are large enough to extend beyond the exit point, the input of seawater from vertical unsaturated infiltration landward of the exit point is important to water table dynamics in the upper part of the swash zone (Hegge and Masselink, 1991; Horn et al., 1998; Turner and Masselink, 2012).

Tidal pumping across the beachface also causes seawater to flow into and out of the beach aquifer (Nielsen, 1990). Over a tidal cycle, the variably-saturated beach volume between the low tide water table and the water table at high tide fills and drains, resulting in the exchange of a volume of water, D_t (Li et al., 1999; process 4 in Fig. 1a). This exchange occurs as seawater flows landward into the beach below the tide level, filling empty pore space as the water table rises. Unsaturated infiltration caused by wave overtopping occurs above of the tide level (Fig. 1a). Thus, seawater that enters the beach by wave swash via the unsaturated infiltration pathway partially fills empty pore space that would otherwise be filled by the rising water table caused by the tide. D_{su} is therefore a component of D_t. It should be noted that D_t as defined does not include continuous intertidal circulation caused by the elevated beach water table. For this reason total intertidal flow through the beach is greater than saltwater exchange related to D_t. The water exchange represented by D_t occurs on the order of a tidal cycle or less. Circulating water due to wave set-up may have a longer or

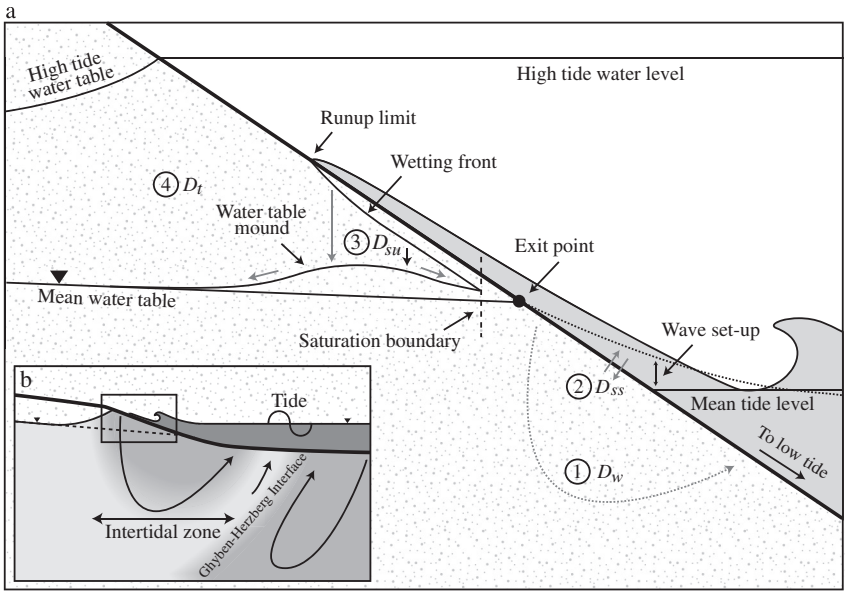

Fig. 1. a) Schematic of beach groundwater and surface water levels. There are four processes related to tides and waves that affect exchange of water between the beach aquifer and coastal waters: (1) wave setup-induced circulation through the saturated subsurface (D_w), (2) swash–groundwater exchange across the lower saturated beach (D_{ss}), (3) swash-induced flow through the unsaturated zone (D_{su}), and (4) tide-driven flux (D_t). Process (3) is a component of (4). Gray arrows denote flowpaths and water exchange pathways. b) Groundwater flowpaths and salinity distribution (white is fresh, gray is saline) in a homogenous coastal aquifer.

shorter residence time depending on wave, beach, and aquifer characteristics.

3. Methodology

3.1. Study sites

This study was conducted on two microtidal sandy beaches at Cape Henlopen, Delaware (Fig. 2). Cape Henlopen, located at the mouth of the Delaware Bay, is a spit complex with a regressive sedimentary sequence. The spit is composed of 12–18 m of very coarse sands, pebbly sands, and gravels overlying shallow marine and estuarine silts and muds (Kraft, 1971). The Cape experiences erosion and shoreline retreat along its Atlantic boundary where sand is transported toward the north and around the tip of the Cape before being redeposited on shallow intertidal sandflats behind the spit (Maurmeyer, 1974). The semidiurnal tides are identical at the two beaches due to their proximity and have a spring tidal range of 1.42 m (NOAA tidal station 8557830, Lewes, Delaware).

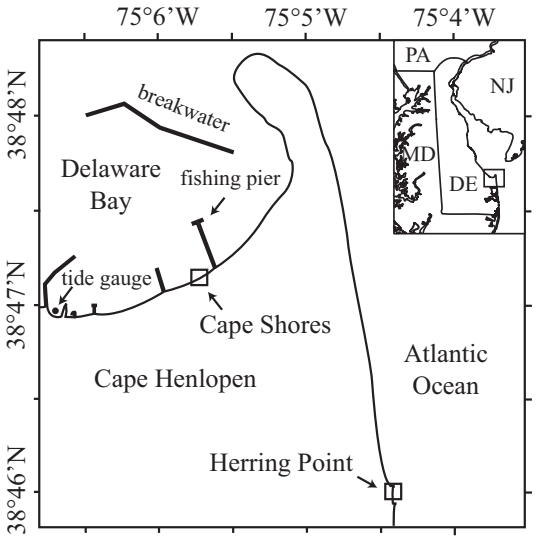

Fig. 2. The Cape Henlopen study area and the exposed Herring Point and sheltered Cape Shores field sites. Herring Point faces directly to the Atlantic Ocean and its waves. Cape Shores is protected from direct wave action by the Cape Henlopen spit complex and by a breakwater.

The two sites were chosen for their contrasting wave conditions and beach morphologies. Herring Point is located on the ocean side of Cape Henlopen and Cape Shores is located on the bay side of the Cape behind a breakwater (Fig. 2). Based on the conditions observed during our field experiments and the criteria of Short (2006), Herring Point is a wave-dominated beach while Cape Shores is a tide-dominated beach. The average beach slope is 0.06 (1:17) at Herring Point and 0.11 (1:9) at Cape Shores. Differences in wave field and sediment grain size lead to a 12 m wide swash zone at Herring Point and a 3 m swash zone at Cape Shores. Swash zone width was constant at each site during the experimental period. The width of the unsaturated beachface within the swash zone was approximately 5 m at Herring Point and 2 m at Cape Shores.

Grain size and hydraulic conductivity were determined from samples taken at three locations across the beachface at each site: mean lower low water (MLLW), mean sea level (MSL), and mean higher high water (MHHW). Grain size analysis was conducted using standard sieving procedures. The range of mean grain size across the beach was 242–679 μm at the Herring Point site and 540–668 μm at the Cape Shores site. Constant-head permeameter tests yielded hydraulic conductivity values of 2.5×10^{-4} m/s, 2.1×10^{-4} m/s, and 2.6×10^{-4} m/s at MLLW, MSL, and MHHW at Herring Point, respectively, and 3.4×10^{-4} m/s, 3.2×10^{-4} m/s, and 3.5×10^{-4} m/s at MLLW, MSL, and MHHW at Cape Shores, respectively. The average hydraulic conductivity of the beaches based on the U.S. Bureau of Reclamation formula (Vukovic and Soro, 1992) is 2.4×10^{-4} m/s for Herring Point and 3.5×10^{-4} m/s for Cape Shores, both of which fall within the range of permeameter estimates.

3.2. Instrumentation and deployment

Moisture sensors and pressure transducers were used to measure volumetric water content and pore pressure within the beach. Measurements were collected at three locations on the beachface at each site: MLLW, MSL, and MHHW for a total of six experimental runs on different dates (Table 1). At each location, four closely spaced, shore-perpendicular instrument arrays were installed, each with three moisture sensors positioned in the unsaturated zone and with a pressure transducer placed below the water table (Fig. 3). The moisture sensors were pushed horizontally into the wall of a hand-augered borehole to ensure that measurements were taken at undisturbed sediment bulk densities. The borehole was backfilled with the excavated sediment which was then compacted to the undisturbed bulk densities of the beach sediment.

Different vertical and horizontal spacings of the moisture sensors were used at the two sites in order to compensate for the different thicknesses of the unsaturated zone and widths of the unsaturated beachface within the swash zone (Fig. 3). The sensors were installed at 46, 131, and 216 mm below the sand surface at Herring Point and 40, 110, and 195 mm below the surface at Cape Shores. The horizontal distances between the vertical instrument arrays were 1.25 m at Herring Point and 0.5 m at Cape Shores.

Instrument cables were buried in a trench away from the instrument transect leading up the beachface to a datalogger (Campbell Scientific CR1000) that synchronously logged data at 5 Hz. Measurements began when the run-up limit was just seaward of the instrumented transect and continued during rising tide until the swash zone migrated up the beachface and over and beyond the instrument arrays.

Volumetric water content (volume of water per volume of bulk sediment) was measured in the unsaturated zone using twelve soil moisture sensors (Decagon Devices EC-5). The sensors measure the dielectric permittivity of the sediment, which is primarily a function of water content. Temperature effects are minor; an uncertainty of up to 2 vol.% can be expected over a temperature range from 5 °C to 40 °C (Bogena et al., 2007; Rosenbaum et al., 2011). The EC-5 sensors were chosen for the small volume of sediment required for measurement. An uncertainty of ±3–4% is expected for most medium to fine-textured sediments containing fresh porewater and up to ±10% for coarse-grained sediments containing saline porewater. To reduce the uncertainty of water content measurements to ±1–2%, site-specific calibrations correcting for sediment texture and porewater salinity were performed. Intertidal sediment samples were collected and oven dried in the laboratory, and then sensor output voltage was recorded as the sediment was exposed to a range of saturation conditions using seawater obtained from the field sites. Gravimetric water content was used to generate linear calibration curves for the sensors at each site.

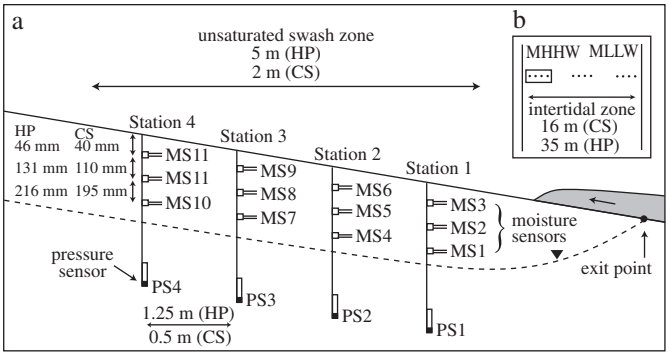

Fig. 3. (a) Cross-sectional schematic of sensor layout used in all of the field experiments. Uniform horizontal spacing was used between sensor arrays at each site, but the spacing was adjusted to account for differences in swash zone width between sites (CS = Cape Shores; HP = Herring Pont; see Fig. 2). The vertical spacing between moisture sensors on each array was also uniform for each deployment across the intertidal zone but differed between sites; (b) Inset shows map view of sensor configuration for the three deployments across the beachface.

Water table elevations were inferred from pore pressure measurements obtained from pressure transducers (Druck PTX 1835). The 4–20 mA transducers have an operating range from 0 to 1517 mbar and an accuracy of 0.10%. Prior to installation, a nylon screen was placed over the pressure port of each sensor to prevent sand grains from contacting and damaging the diaphragm, and the area between the diaphragm and the screen was filled with seawater to purge air pockets.

The use of point measurements of pore pressure to infer water table elevations may not be valid in the presence of vertical flow caused by vertical hydraulic gradients. A manometer attached to a nested piezometer with two 1 cm screens 40 cm apart was used to observe vertical hydraulic head differences within the saturated aquifer beneath the swash zone. At both sites, the head difference was always ≤1.5 mm, which is within the measurement error of our pressure transducers and much less than the measured fluctuations in hydraulic head.

The wave heights at Herring Point (0.50 m) and Cape Shores (0.11 m) were measured during the MLLW deployments when the offshore significant wave height was 1.41 m as measured by National Buoy Data Center buoy #44009 located at the mouth of the Delaware Bay. Offshore significant wave heights during all other deployments were within 7 cm of this value, indicating that wave conditions were similar between deployments at each site (Table 1).

3.3. Calculated wave setup (D_w) and variably-saturated tidal exchange (D_t)

The analytical model in Li et al. (1999) is used to estimate the tidally controlled variably-saturated beach volume (D_t). While this model is simplified and approximate, it is used to put our calculated unsaturated swash infiltration rates (D_{su}; Section 4.3) into context. As discussed in Section 2, D_{su} is a component of D_t. Thus D_t was also calculated for both sites to determine the approximate proportion of seawater that is contributed by D_{su} to D_t. An expression for the discharge rate per alongshore distance associated with D_t is given by Li et al. (1999) as:

$$D_t = \frac{n_e A}{\kappa T_t}\exp(-\alpha)[\cos(\alpha) - \sin(\alpha)] + \frac{\sqrt{2}n_e A^2}{s_b T_t}\exp\left(-\sqrt{2}\alpha\right)\cos\left(\sqrt{2}\alpha\right) + \frac{n_e A^2}{s_b T_t} \quad (1)$$

with

$$\kappa = \sqrt{\frac{n_e \omega}{2KH}} \quad (2)$$

and

$$\alpha = \frac{\kappa A}{s_b} \quad (3)$$

where n_e is the effective porosity, A is the tidal amplitude, T_t is the tidal period, σ is the breaking index, s_b is the beach slope, ω is the wave frequency, K is the hydraulic conductivity, H is the average aquifer thickness, and κ is the wave number.

We also calculate the discharge rate driven by the steady onshore hydraulic gradient that results from wave set-up, D_w (Li et al., 1999):

$$D_w = Ks_wL \tag{4}$$

where D_w is the discharge rate per unit alongshore distance, K is the hydraulic conductivity, s_w is the slope of wave setup, and L is the distance between the breaker line and the run-up line. The values of s_w and L can be calculated from local wave and beach conditions:

$$s_w = \frac{3\sigma^2 s_b}{8 + 3\sigma^2} \tag{5}$$

and

$$L = \frac{H_b}{\sigma(s_b - s_w)} \tag{6}$$

where H_b is the breaker height, s_b is the beach slope, and σ is the breaking index, given by:

$$\sigma = \frac{1.56}{1 + \exp(-19.5s_b)} - 43.8[1 - \exp(-19s_b)]\frac{H_b}{gT_w^2} \tag{7}$$

where g is gravitational acceleration and T_w is the wave period.

The parameters used to estimate wave setup and variably-saturated tidally driven fluxes are shown in Table 2. The breaker height, wave period and beach slope were measured in the field. The effective porosity was taken from the moisture sensor measurements at the end of the experimental runs. The hydraulic conductivity was the average of the values determined from the permeameter tests (see Section 2.1). The tidal amplitude and period were determined from the nearby tide gauge station. We also present a range of values for model parameters that vary in time or space. These are breaker height, wave period, tidal amplitude, beach slope, effective porosity, hydraulic conductivity, and aquifer thickness. The observed minimum and maximum values and the values used in calculations are given in Table 2.

4. Results

4.1. Swash-driven moisture dynamics

Water content and water table elevations show a complex response to wave overtopping. Data from the Herring Point and Cape Shores MHHW experimental runs are shown in Fig. 4. Time series from the remaining three stations and other four

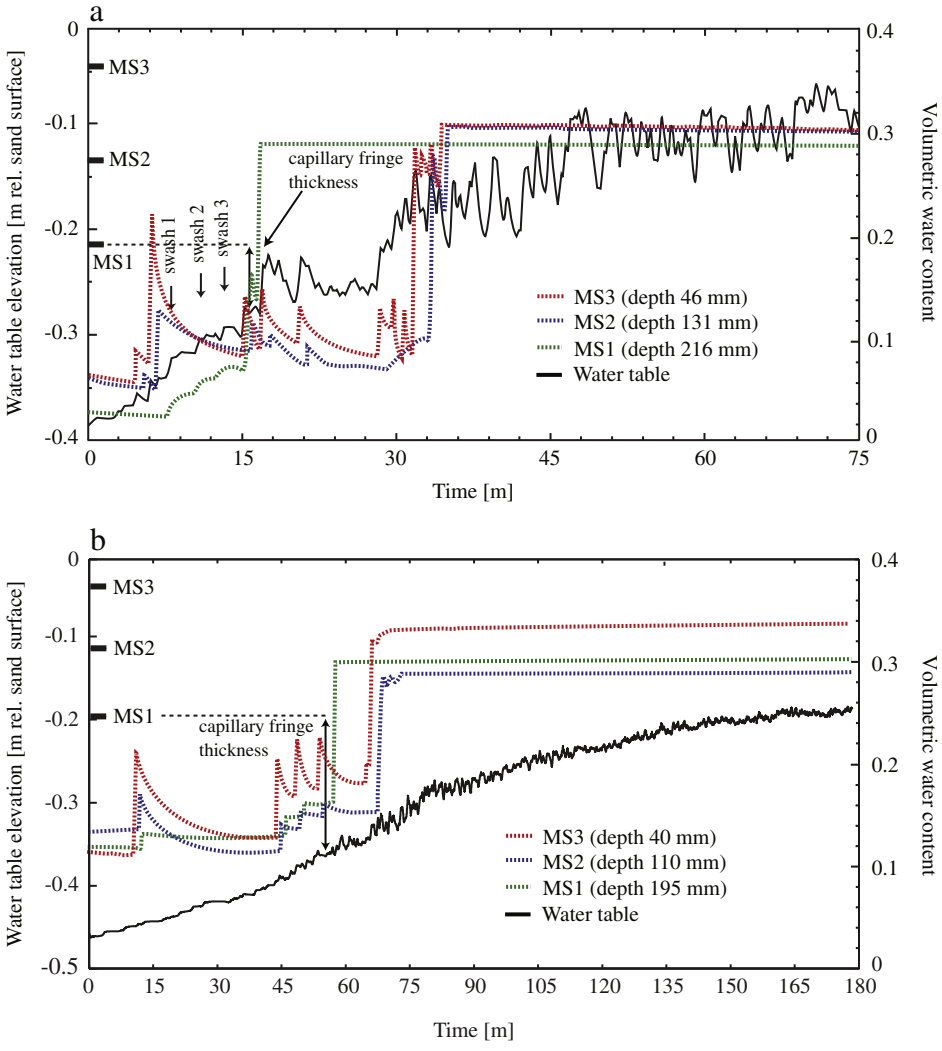

Fig. 4. Station 1 time series of water table elevation relative to the sand surface and volumetric water content measured at three depth intervals below the sand surface at a) Herring Point and b) Cape Shores near MHHW. Tick marks denote elevation of each moisture sensor relative to the sand surface. Note that moisture conditions are expressed as volumetric water content: saturated conditions correspond to water content that is equivalent to the porosity of the sediment (~0.3 at our sites). It is important to note that these data are from the MHHW stations, a zone which is very infrequently inundated. The potentiometric surface is therefore always below the sand surface.

experimental runs show a similar response to wave run-up and run-down and are shown in the Supplementary Material.

Water content in the shallow subsurface responded rapidly, but asymmetrically to wave swash. Upon wave overtopping, water content in the upper part of the unsaturated zone rose rapidly and, after swash run-down, gradually declined (Fig. 4). Water content in the mid and shallow depths responded similarly to each swash cycle. Saturation (water content equal to porosity) by wave swash occurred downward from the initially unsaturated sand surface to the deeper sediments. At depth, the initial effects of swash penetration were not apparent. Saturation of the deepest sensor generally occurred due to a rise in the local water table, rather than by downward saturation from the surface. The deepest moisture sensor consistently saturated first, followed by the shallowest sensor and then the middle sensor.

Saturation occurred more rapidly at the MSL sites than at the MHHW and MLLW sites. The average time from first wave overtopping to saturation at each station at Herring Point during the MSL experiment was approximately 28 min compared to 33 and 38 min at MHHW and MLLW, respectively. Similarly, saturation occurred 28 min after the first wave overtopping during the MSL experiment at Cape Shores. This is in contrast to the MHHW and MLLW experiments at Cape Shores, where an average of 65 and 42 min of wave overtopping at each station was required to saturate the beach sediments, respectively. These observations are likely the result of the rate of tidal rise; this rate is highest at mid-flood tide (when the MSL experiments were conducted) than at the beginning or end of flood tide (when the MLLW and MHHW experiments were conducted).

The amplitude of the water content response to swash infiltration varied with depth and time. Fig. 4 shows that the amplitude of water content fluctuations in the intermediate depths of the unsaturated zone (MS2) at Herring Point and Cape Shores were dampened relative to those closer to the surface. This suggests that once the swash recedes and infiltration ends, much of the infiltrated water is retained in the upper third of the unsaturated zone. While the amplitudes of the swash responses in the upper unsaturated zone were similar at the two sites in this example (Fig. 4), the amplitude measured by the middle moisture sensors (MS2) at Cape Shores was smaller than those at Herring Point. The water table response to wave overtopping was also significantly larger at Herring Point than Cape Shores, where at times there was no movement of the water table in response to swash infiltration. These observations are consistent with the smaller influxes per swash cycle at Cape Shores, which limit infiltration to the midsection of the unsaturated zone and the water table.

4.2. Water content profiles

The moisture sensors were used to map water content conditions in the unsaturated zone. Previous estimates of vertical movement of water into beach aquifers considered a sharp air/water interface (i.e. wetting front) and saturated flow (e.g. Horn et al., 1998; Horn and Li, 2006; Austin and Masselink, 2006; Steenhauer et al., 2012). However, our observations indicate that infiltration can occur as partially saturated flow. The time series of water content, such as the example in Fig. 4a, were used to infer the vertical location of the partially saturated front and wetting front at various times during field experiments. For the Herring Point MHHW experiment (Fig. 4a), water content increased at all sensors following the first major swash event at 6.5 min. However, the measurements show that saturation was never achieved as would be expected by the passage of a saturated wetting front.

Fig. 5 schematically illustrates the process of swash infiltration based on our observations. Initially, as the tide rises and the swash

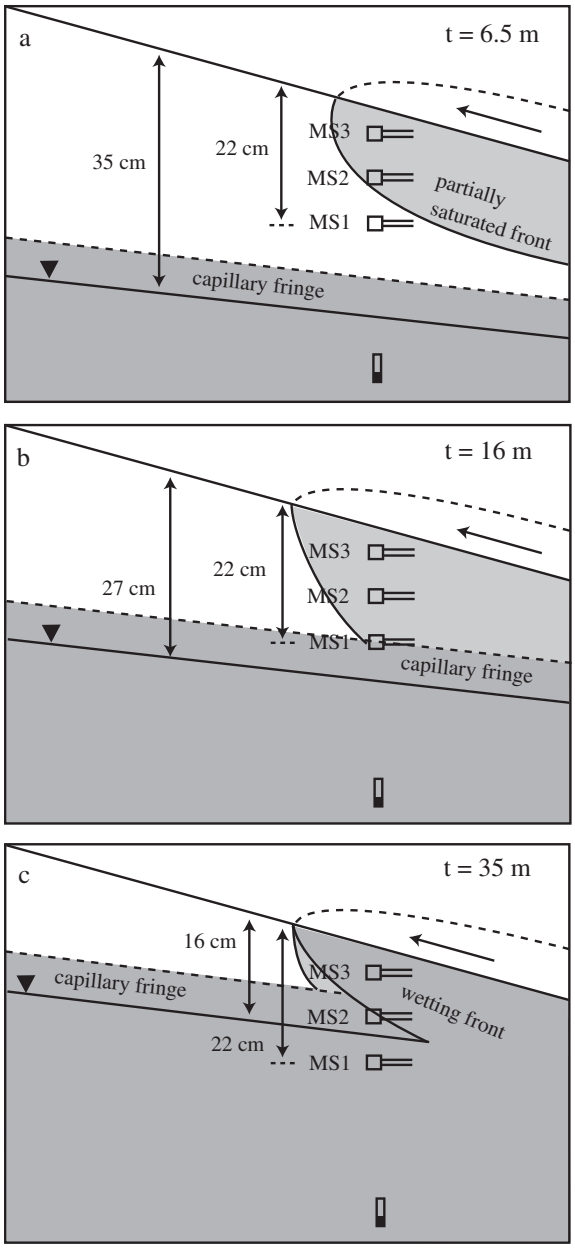

Fig. 5. Distribution of water content in the swash zone with location of the partially saturated front, wetting front, water table relative to the sand surface at Station 1 at the Herring Point site near MHHW. Light gray shading denotes partially saturated conditions and dark gray shading denotes fully saturated conditions. Dashed line above land surface indicates inferred position of wave swash, and dashed line above water table indicates inferred position of the top of the capillary fringe.

first overtops a section of the beach (equivalent to the event at 6.5 min at Herring Point discussed above), a partially saturated front migrates vertically into the beach aquifer with small impact on the water table below (Fig. 5a). After additional swash events and an increase in tide level (equivalent to the conditions at 15 min observed at Herring Point; Fig. 4a), the upper part of the beach aquifer increases in saturation, while the rise in the water table and capillary fringe leads to saturation of the deepest sensor (Fig. 5b). At 35 min, all moisture sensors recorded saturated conditions (Fig. 4a). The top sensor saturated immediately before the middle sensor, suggesting that the shallow sensors are behind the fully saturated wetting front (Fig. 5c). The deepest sensor is below the water table (Fig. 5c).

4.3. Calculations and estimates of unsaturated swash infiltration

The swash-driven unsaturated infiltration rate, D_{su}, was estimated using volumetric water content profiles from the vertical arrays of moisture sensors. Since changes in saturation were observed first at the shallowest sensor (MS3) and water content consistently declined at the upper sensor before rising at the middle sensor (MS2), we can assume that once MS3 began to decline, the slug of infiltrating seawater was fully contained in the region extending from the sand surface to the depth of MS2. This is based on the assumption that a reduction in water content at MS3 occurred after the swash receded, infiltration ceased, and the sand surface became subaerial. Thus, the volume of seawater that entered the beach over a swash cycle at a particular station can be calculated as the difference between the vertical water content profile immediately before the water content at the shallowest sensor (MS3) began to increase, defined as $T1$, and the time at which MS3 peaked, defined as $T2$. Two example profiles at $T1$ and $T2$ at Herring Point and Cape Shores are shown in Fig. 6. Assuming that the observation point was inundated just before $T2$, the sand surface was presumed to be saturated at $T2$ ($\sim$0.3 as measured by the moisture sensors under saturated conditions; see Fig. 4). The water mass was assumed to extend vertically from the sand surface to the depth of MS2 based on the observation that water content at MS2 consistently began to rise moments after $T2$ for all cases where MS2 responds to individual swash events. As a result of these assumptions, the calculated infiltrated water volume should be considered an upper bound, since it is possible that at $T2$, saturation had begun to decrease at the land surface or the infiltrating water mass had not yet reached MS2. However, for the reasons discussed above, we believe that this discrepancy is small. In future studies, additional moisture sensors may be used to more precisely delineate the infiltrating water mass.

In order to calculate the infiltration rate, functions were fit to data at $T1$ and $T2$. An exponential function was fit to measurements at $T2$ based on the observation that when MS3 was not saturated, water content at $T2$ decreased rapidly from MS3 to MS2 and then leveled off from MS2 to MS1 (Fig. 6). The water content profile at $T1$ was assumed linear between MS2, MS3, and the sediment surface. This assumption was consistent with measurements of water content at all three sensor locations (Fig. 6a), except in some cases where water content at MS1 was higher, likely due to proximity to the water table and saturation from below (e.g., Fig. 6b).

The swash-driven unsaturated infiltration volume, D_{su}, over a swash cycle at an instrument array is then calculated as:

$$D_s = \int_{-Z_{MS2}}^{0} S_{T2}(z)\mathrm{d}z - \int_{-Z_{MS2}}^{0} S_{T1}(z)\mathrm{d}z \tag{9}$$

where $S_{T2}(z)$ is the water content S as a function of depth z at $T2$, $S_{T1}(z)$ is the water content as a function of depth at $T1$, and Z_{MS2} is the depth of MS2 relative to the sand surface. The shaded gray region in Fig. 6 represents the volumetric change in water content due to wave overtopping calculated using equation (9).

Equation (9) can be used to calculate infiltration rates over four spatial and temporal scales: infiltration per swash event (cm/swash) at each station, infiltration over a tidal cycle at each station (m^3/m^2/tidal cycle), total infiltration (m^3/m^2/tidal cycle) in the swash zone at MHHW, MSL, and MLLW, and cumulative infiltration across the beach over a tidal cycle (m^3/m length of shoreline/tidal cycle).

Infiltration due to individual swash events that inundated the beach aquifer varied between stations and with time at each station (Fig. 7). The volume of seawater that entered the beaches with each swash was generally largest after the first wave overtopping followed by a decrease in infiltration with subsequent waves until the swash infiltration event that resulted in full saturation. In all cases, infiltration increased significantly during the final swash event that saturated the swash zone. The final rate of infiltration was often comparable to the volume of seawater that entered the beach from the first wave (Fig. 7). This final increase in water content may be the result of simultaneous tidal inundation and swash infiltration.

The volume of seawater that infiltrated over the tidal cycle due to swash was generally uniform across the unsaturated swash zone.

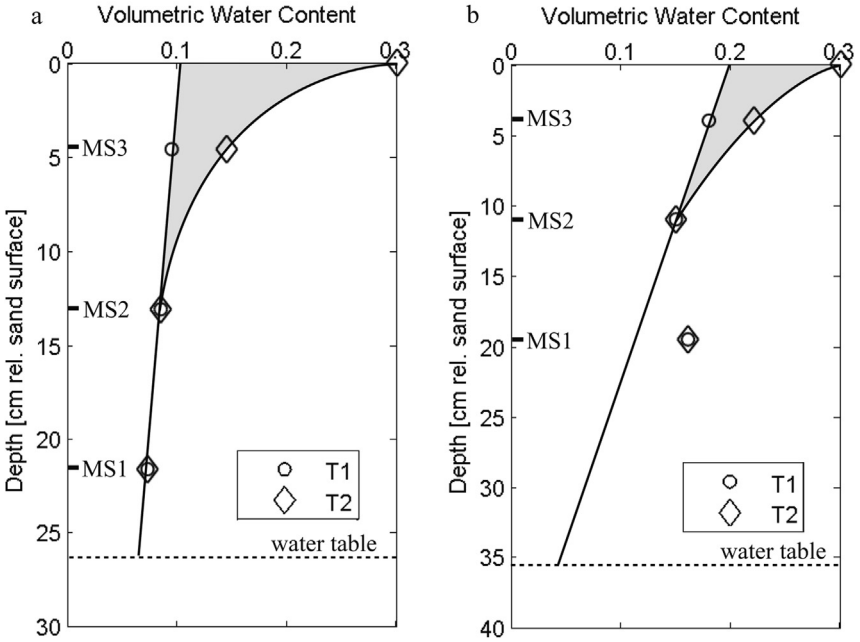

Fig. 6. Water content profile before ($T1$) and after ($T2$) a swash event that occurred at Station 1 during the MHHW experiment at a) Herring Point and b) Cape Shores. Shaded area represents the change in volumetric water content from $T1$ to $T2$.

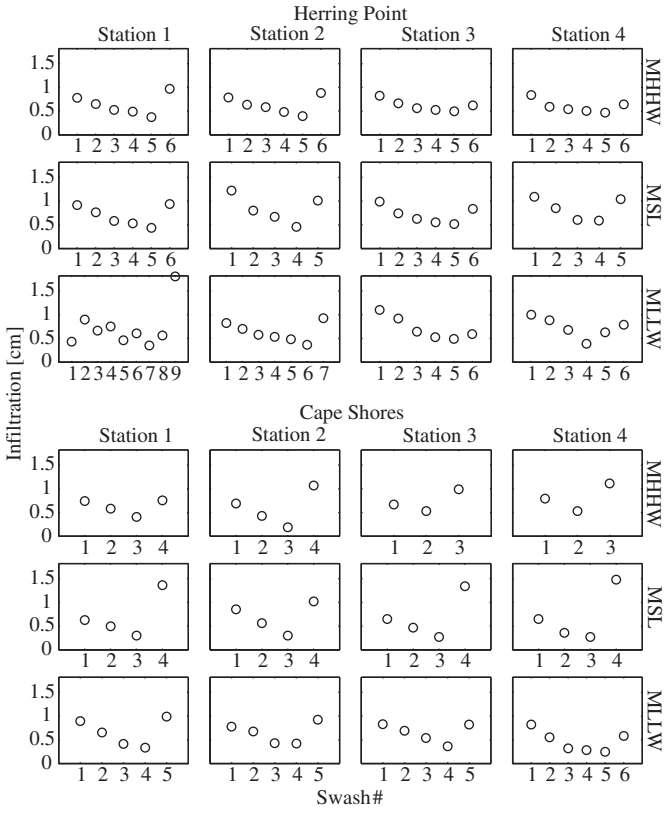

Fig. 7. Unsaturated infiltration per swash event at each station during the MLLW, MSL, and MLLW deployments at Herring Point and Cape Shores.

Table 1 shows infiltration rates at all stations across both beaches over a tidal cycle. The minor differences between stations are likely due to small-scale variability in hydraulic conductivity and porosity. The effect of this heterogeneity is much less than the difference in infiltration between low and high tide.

Total unsaturated infiltration into the swash zone increased up the beachface from low to high tide at both sites (Table 1). Infiltration at mid tide at Herring Point was 86% of that at high tide. At low tide, inflow was less with a rate equal to 76% of the high tide flux. Cape Shores experienced a similar decreasing trend where 90% and 76% of the high tide flux was observed at mid and low tide, respectively.

The cumulative volume of seawater that entered the beach due to wave swash across the unsaturated flow pathway over a tidal cycle was calculated by integrating a regression line fit to the average infiltration rate at low, mid, and high tide over the distance from MHHW to MLLW. Cumulative swash infiltration over a tidal cycle across the beachface at Herring Point was significantly greater than at Cape Shores. A total of 1.6 m^3 of seawater entered the beach at the wave-dominated Herring Point site while 0.4 m^3 infiltrated into the tide-dominated Cape Shores beach.

4.4. Horizontal hydraulic gradients

Saturated pore pressure measurements were used to calculate horizontal hydraulic gradients across the instrument transect in the swash zone during a rising tide. The time-averaged effect of event-driven infiltration through the unsaturated zone is the formation of a groundwater mound above the mean water table elevation (Kang et al., 1994). The mounding results in a groundwater divide from which water flows in both the landward (negative gradient in Fig. 8) and seaward (positive gradient in Fig. 8) directions. We used the hydraulic gradients between the closely spaced pressure transducers to track the position of the mound across the beach at the time scale of wave swash as the swash zone and tide migrated up the beach (Fig. 8). The position of the mound is the point at which the gradient transitions from negative to positive between adjacent stations. As the tide rose across MHHW at Herring Point, the mound passed between stations 1 and 2 at 60 min, between 2 and 3 at 90 min and between 3 and 4 at 110 min (Fig. 8a–c, respectively). At the Cape Shores site, gradients were primarily positive indicating that the size of the groundwater mound, although present, was not large enough to overcome the larger-scale intertidal gradient to reverse the flow direction, as was the case at Herring Point (Fig. 8e–h and d). Nonetheless, the small mound temporarily reduced seaward flow driven by the terrestrial gradient as the mound migrated from stations 1 to 4 between 90 and 120 min. The higher beach slope and lower wave intensity at Cape Shores led to a significantly different subsurface flow regime compared to Herring Point.

Landward groundwater flow velocities were calculated using the maximum horizontal hydraulic gradients and the hydraulic conductivity and porosity at the observation point. At both sites, the maximum flow rates were observed during the MHHW experiments. Horizontal flow velocities determined from the gradient between the farthest seaward and farthest landward pressure transducers (PS1 and PS4; Fig. 8d and h) were 3.8 m/d at Herring Point, whereas a velocity of nearly zero was observed at Cape Shores. Smaller-scale gradients between adjacent sensors indicate maximum velocities of 5.6 m/d at Herring Point and 4.0 m/d at Cape Shores, both at the lower end of the swash zone during the MHHW experiment.

At Cape Shores, the positive (seaward flow) and negative (landward flow) hydraulic gradients related to the mound (Fig. 8h) can be compared to the larger-scale terrestrial hydraulic gradient. The maximum terrestrial hydraulic gradient measured at the site is approximately 0.024 ± 0.005 (Ullman et al., 2003). This is less than the largest positive gradient across the mound, 0.06. Thus, infiltration locally strengthened the terrestrial gradient on the seaward side of the mound and increased seaward flow. The opposite was the case on the landward side of the mound where infiltration

Table 1
Unsaturated infiltration across the swash zone [cm^3/cm^2/tidal cycle] unless otherwise specified. Swash zone width as shown in Fig. 3.

Location	Date	Sig. wave height [m]	Beach slope	Station 1	Station 2	Station 3	Station 4	Total [cm^3/swash zone width/tidal cycle]
HP MLLW	2/18/2011	1.41	0.06	3.8	3.8	3.7	3.6	18.6
HP MSL	8/5/2011	1.40	0.06	4.2	4.2	4.2	4.2	20.9
HP MHHW	4/20/2011	1.41	0.06	6.4	4.4	4.3	4.4	24.5
CS MLLW	1/19/2011	1.41	0.11	2.5	2.4	2.2	2.4	4.7
CS MSL	10/27/2011	1.34	0.11	2.8	2.7	2.7	2.8	5.5
CS MHHW	4/21/2011	1.36	0.11	3.3	3.2	3.2	2.8	6.3

HP Herring Point
CS Cape Shores.

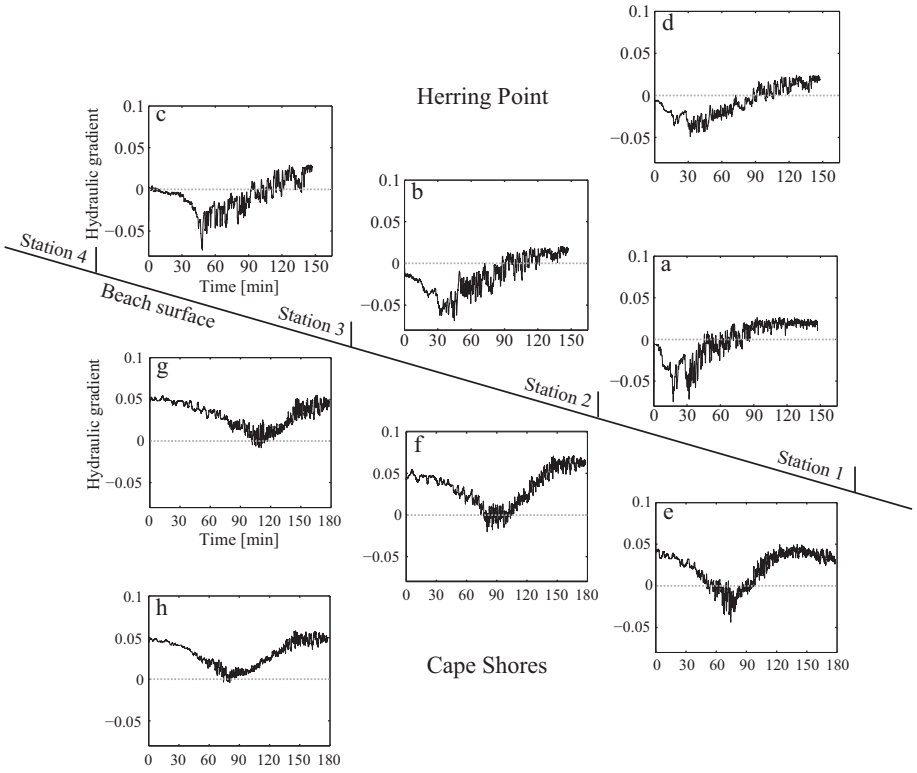

Fig. 8. Hydraulic gradients between stations 1 and 2 (a and e) stations 2 and 3 (b and f) stations 3 and 4 (c and g) and stations 1 and 4 (d and h) during rising tide near the high tide mark at the Herring Point and Cape Shores study sites (data from MHHW deployments). The time is relative to the arrival of the top of the swash zone at Station 1. Positive gradient corresponds to flow in the off-shore direction and negative gradients correspond to the on-shore direction.

reduced the terrestrial gradient to zero, locally halting flow toward the sea.

5. Discussion

5.1. Water content response characteristics

Although water content had previously not been measured in the unsaturated zone, field studies demonstrate that pressure within this zone fluctuates in response to wave swash. These pressure fluctuations are similar to the moisture fluctuations observed in this study, as expected considering that pressure and water content co-vary (Van Genuchten 1980). Both water content and pressure (e.g. Turner and Nielsen, 1997; Horn et al., 1998; Baldock et al., 2001; Cartwright et al., 2006) increase rapidly in response to wave overtopping and then decline at a slower rate during run-down. This type of pressure behavior can occur in regions landward of the run-up limit of individual swash events as a result of the inland propagation of a pore pressure wave (Waddell, 1976; Hegge and Masselink, 1991; Horn et al., 1998; Baldock et al., 2001; Cartwright et al., 2006). Our findings provide insight into the volumes and rates of groundwater flow that are driven by the hydraulic gradients that result from these pressure fluctuations.

The magnitude of the water content fluctuation from wave swash is dependent on the water content of the beach immediately prior to the arrival of each wave. High initial water content conditions reduce available pore space for infiltrating seawater, thereby reducing the magnitude of the water content fluctuation. At the early stages of each experiment, the water content of the beach aquifer was relatively low, hence larger volumes of seawater were able to flow into the beach early in each experiment (Fig. 7). Conversely, water content was generally higher towards the end of the experiments before saturation, which resulted in a general reduction in inflow with time.

Swash events that do not overtop the observation points still have an effect on the pore pressures at those locations, consistent with observations by Waddell (1976), Horn et al. (1998), Baldock et al. (2001), and Cartwright et al. (2006). For example, the three events labeled Swash 1, 2, and 3 in Fig. 4a caused the water table to rise and fall at Herring Point, while there was no observable response of water content in the shallow sediment surrounding MS2 and MS3. This suggests that the sand surface at the observation point did not become inundated during wave run-up and that the water table response was due to the inland propagation of a pore pressure wave originating from a point farther seaward. The narrow range of these pressure fluctuations suggests that the water table exit point was significantly seaward of the measurement location (e.g. Cartwright et al., 2006). However, this cannot be confirmed because the position of the exit point was not monitored in this study. Pressure fluctuations landward of the run-up limit have been observed previously (e.g. Cartwright et al., 2006), but the response of water content to these fluctuations has not been examined at swash frequencies. The simultaneous measurements of moisture and pressure in this study allows for such an analysis. The movement of the water table appears to have invoked a simultaneous response in the water content measured by the deepest moisture sensor, located approximately 10 cm above the water table (see moisture responses at Swash 1, 2, and 3 in Fig. 4a). This indicates that water content above the capillary fringe in the unsaturated zone can respond to rapid changes in water table elevation. Thus, the influence of wave swash on water content and flow in the unsaturated zone extends beyond the width of the swash zone.

5.2. Unsaturated infiltration

5.2.1. Assumptions and explanations of infiltration estimates

The calculation used to estimate cumulative infiltration requires simplifying assumptions. First, we assume that infiltration increased linearly up the beach between measurement locations. However, the presence of small-scale heterogeneities between the observation points would likely result in a non-linear trend. Second, we assume that the width of the swash zone remained constant during the tidal cycle, which requires that the slope of the beach was uniform across the intertidal zone and that wave conditions were constant over the tidal cycle. Our measurements show that both of these requisites were met (Table 1). Third, we assume a constant width of the intertidal zone. For Herring Point and Cape Shores, the width of the intertidal zone that was used in the calculation was the average of the three widths that were measured during each of the three experiments at the two sites. A wider (narrower) intertidal zone would likely result in a higher (smaller) cumulative infiltration estimate due to a larger (smaller) intertidal unsaturated pore volume available for inflow.

Although measurements were collected only during rising tide, results are presented as infiltration over a tidal cycle based on the assumption that negligible flow into the beach occurs during falling tide. When the rate of tidal fall exceeds the rate of water table fall during ebb tide, an outcropping of the water table (i.e. seepage face) will form and exfiltration will occur in the vicinity of the swash zone (Turner, 1993b). The presence of moisture above the water table in the capillary fringe will reduce the drainage capacity of the beach and increase the size of the seepage face (Naba et al., 2002). Combined with this drainable moisture above the water table and a rapidly falling tide, seepage faces are common at the two sites. During rising tide, it is reasonable to assume that the elevation of the tide is equal to the elevation of the water table (Turner, 1993b) and that swash events that extend onto the unsaturated zone will drive greater flow into the subsurface than during ebb tide (Kang et al., 1994). Calculated rates based on our measurements are therefore taken as the total quantity of seawater that entered the beach over a tidal cycle.

The pattern of increasing infiltration from low to high tide requires explanation. The slope of the beach at MHHW, MSL, and MLLW was constant across each beach, as were offshore wave conditions (Table 1). Therefore the rise in infiltration from low to high tide was likely not due to a widening of the swash zone up the beach. The inflow behavior can instead likely be explained by a thickening of the tidally unsaturated zone with distance up the beach. The depth to the water table across both beaches was lowest near low tide and reached a maximum near the high tide mark. A deep water table supports a greater volume of unsaturated interstitial pore space to be filled and drained over a tidal cycle than a shallow one. Consequently, the highest inflow volumes were observed at high tide while infiltration was lowest near low tide.

The cumulative volume of seawater that entered the beach at Herring Point through swash was greater than that at Cape Shores due, in part, to a wider intertidal zone that is a result of a lower beach slope. The similarity in hydraulic conductivity at the sites (see Section 3.1) suggests that the differences in infiltration were not the result of differences in sediment permeability. Instead, the 35 m wide intertidal zone at Herring Point allowed for infiltration to occur over a greater area than that across the 16 m intertidal zone at Cape Shores. Even if the intertidal zones at the two sites were of equal width, the cumulative infiltration rate due to swash would likely remain higher at Herring Point due to a wider swash zone resulting from higher wave heights. However, it is also important to consider that the movement of a fast tide across a gentle sloping and low conductivity beach (Herring Point) can lead to a large seepage face (Li et al., 2008), which could reduce the size of the unsaturated beachface in the swash zone, thus reducing unsaturated infiltration. The opposite might be expected for Cape Shores, where a smaller seepage face might be anticipated due to a slower moving tide, resulting in higher unsaturated infiltration rates caused by a larger unsaturated sand surface in the swash zone. Nonetheless, the effect of seepage face development on unsaturated swash infiltration appears to have been less important than the difference between wave conditions at the study sites. Other factors, such as swash depth, period, and permeability may also significantly affect unsaturated swash infiltration.

5.2.2. Measured vs. modeled infiltration

The volume of pore space between the water table at high tide and the water table at low tide (D_t) and the circulation of saltwater caused by wave set-up (D_w) were calculated to compare with our estimates of unsaturated infiltration (Table 2). As discussed in Section 2, D_t does not include continuous tidally driven circulation through the beach, so total intertidal flow is greater than the combined D_t and D_w flux. However, since D_{su} is a component of D_t (see Section 2), we estimate the percent of D_t contributed by D_{su} as the ratio of measured unsaturated infiltration over a tidal cycle to the pore volume between the high and low tide water table levels as approximated by Equation (1) (Table 2). Unsaturated swash infiltration is responsible for filling approximately 62% of the D_t volume at Herring Point (with a lower beach slope and higher wave amplitude), and 13% at Cape Shores (with a higher beach slope and lower wave amplitude; Table 2). The relative importance of wave swash is undoubtedly influenced by the differences in wave height, beach slope, and width of the intertidal zone. Of the three saltwater exchange pathways that we considered (D_t, D_w, and D_{su}), D_{su}

Table 2
Parameter and calculated values of groundwater seepage due to waves and tides at Herring Point and Cape Shores.

Parameter	Herring Point			Cape Shores		
	Min value	Max value	Best estimate	Min value	Max value	Best estimate
H_b [m]	0.2	1	0.5	0.05	0.13	0.11
T_w [s]	4	12	8	1.8	5	3.4
s_b	0.05	0.07	0.06	0.1	0.13	0.115
K [m s^{-1}]	2.07×10^{-4}	2.55×10^{-4}	2.38×10^{-4}	2.52×10^{-4}	3.41×10^{-4}	3.05×10^{-4}
η_e	0.2	0.4	0.3	0.2	0.4	0.3
A [m]	0.61	0.89	0.71	0.61	0.89	0.71
T [s]	44,700	44,700	44,700	44,700	44,700	44,700
H [m]	40	60	50	40	60	50
D_t [m^3 tidal cycle^{-1}] (Eq. (1))	1.5	4.2	2.6	1.7	5.1	3.0
D_w [m^3 tidal cycle^{-1}] (Eq. (4))	0.4	2.6	1.1	0.1	0.9	0.4
D_{su} [m^3 tidal cycle^{-1}] (measured)	–	–	1.6	–	–	0.4
D_t contributed by D_{su}			62%			13%

differed the most between the two sites, with Cape Shores experiencing 75% less swash infiltration than Herring Point. This may in part be caused by the differences in wave height at the two sites: breaker wave heights at Cape Shores were 78% less than breaker heights at Herring Point. At both sites, wave swash may drive seawater into the unsaturated zone in quantities that are comparable to fluxes driven by the steady hydraulic gradient from wave setup. Flow through the unsaturated swash pathway is 1.5 times higher than modeled estimates of wave setup-driven flux at Herring Point while the two fluxes are approximately equal at Cape Shores (Table 2). The results suggest that fluxes associated with unsaturated swash infiltration can be significant in certain settings and should be considered when evaluating the importance of waves and tides in driving seawater into the beach aquifer.

5.3. *Implications: horizontal hydraulic gradients beneath the swash zone*

The temporal and spatial variability in horizontal flow direction in the intertidal zone has implications for quantifying the transfer of solutes across the aquifer–ocean interface (Boufadel et al., 2007; Brovelli et al., 2007; Boufadel et al., 2011; Bakhtyar et al., 2013). First, the dynamic water table gradients observed at our sites are likely to affect the distribution of marine organic matter entering the beach through wave swash; this organic matter can remineralize at the water table and modify the chemistry of the beach aquifer (Charbonnier et al., 2013). Second, the location and timing of a contaminant spill on a sandy beach under the influence of waves will dictate the fate of the contaminant as it infiltrates into the beach aquifer (Boufadel et al., 2007; Bakhtyar et al., 2013). Chemicals located near the upper unsaturated region of the swash zone on the landward side of the water table mound may experience localized inland flow despite larger scale seaward flow related to the terrestrial hydraulic gradient. The landward movement of the water table mound brought on by a rising tide may further transport the contaminant up the beach. In addition, the reversing directions of flow resulting from swash infiltration and mounding may increase chemical residence times (Boufadel et al., 2007) and enhance mixing in the beach aquifer before discharge, important factors controlling the fate of reactive contaminants. The formation and transient behavior of the water table mound should therefore be considered when modeling chemical transport within sandy beaches.

6. Conclusions

Field measurements of wave-induced fluctuations in pressure and water content in two sandy beaches provide insights into the effects of wave action and swash infiltration on beach aquifers. Water content in the unsaturated region of the swash zone fluctuated on the time scale of individual wave events in response to wave overtopping, with a rapid rise of water content followed by slower decline. Water content in the mid to shallow region of the unsaturated zone generally increased from the first occurrence of wave overtopping until saturation, although at a slower rate after the initial input. Saturation by wave swash occurred downward from the initially unsaturated sand surface to the mid-section of the unsaturated zone. Saturation of deeper sediment also occurred due to a rise in the water table with rising tide.

Changes in water content were used to estimate swash-driven infiltration across the unsaturated beachface. Swash infiltration was largely uniform across the swash zone but was correlated to tidal stage; rates increased from low to high tide at both study sites due to the increase in pore volume available. Infiltration per meter length of shoreline over a tidal cycle also differed at the two sites, with 1.6 m^3 of seawater entering the wave-dominated Herring Point beach and 0.4 m^3 infiltrating into the tide-dominated Cape Shores beach. This difference is likely related to wave height and width of the intertidal zone.

Field measurements of unsaturated swash infiltration and theoretical estimates of tidal and wave setup driven flux show that swash infiltration filled ~62% of variably-saturated pore space between the high and low tide water tables at the wave-dominated beach and ~13% at the tide-dominated beach. The unsaturated flow driven by swash infiltration may be comparable to flow rates due to other driving mechanisms such as wave setup and tides.

Water content in the unsaturated zone is responsive to wave swash, and flow through this zone contributes to a rising water table and dynamic horizontal hydraulic gradients. These gradients drive flow both onshore and offshore with the spatial extent and migration of these flows controlled by tidal shifts in the location of the swash zone.

Measurements of the physical dynamics of moisture and pore pressure in beach aquifers in response to wave swash and tidal forcing provide insights into the mechanisms that drive infiltration and circulation of seawater in beach aquifer systems. The unsaturated flow pathway and the corresponding residence times may lead to biogeochemical alterations of solutes that differ from those occurring along saturated flowpaths associated with wave set-up and tidally driven flows. Thus unsaturated infiltration is likely important to beach reactivity and the discharge of land-derived chemicals to the coastal ocean. The results demonstrate the complexity of swash–aquifer interactions and highlight the need to consider the magnitude of fluxes associated with unsaturated swash infiltration as well as the temporal and spatial influence of wave swash on water table dynamics over various timescales when understanding groundwater flow dynamics in beach aquifers.

Acknowledgments

This research was supported by the National Science Foundation (NSF) Grant EAR-1246554 and by Delaware EPSCoR with funds from NSF Grant EPS-0814251 and the State of Delaware. We thank the two anonymous reviewers for helpful suggestions that greatly improved the manuscript.

Appendix A. Supplementary data

Supplementary data related to this article can be found at http://dx.doi.org/10.1016/j.ecss.2014.03.015.

References

Austin, M.J., Masselink, G., 2006. Swash–groundwater interaction on a steep gravel beach. Cont. Shelf Res. 20, 2503–2519.

Bakhtyar, R., Brovelli, A., Barry, D.A., Robinson, C., Li, L., 2013. Transport of variable-density solute plumes in beach aquifers in response to oceanic forcing. Adv. Water Resour. 53, 208–224. http://dx.doi.org/10.1016/j.advwatres.2012.11.009.

Baldock, T.E., Baird, A.J., Horn, D.P., Mason, T., 2001. Measurements and modeling of swash-induced pressure gradients in the surface layers of a sand beach. J. Geophys. Res. 106, 2653–2666.

Boehm, A.B., Paytan, A., Shellenbarger, G.G., Davis, K.A., 2006. Composition and flux of groundwater from a California beach aquifer: Implications for nutrient supply to the surf zone. Cont. Shelf Res. 26, 269–282. http://dx.doi.org/10.1016/j.csr.2005.11.008.

Bogena, H.R., Huisman, J.A., Oberdörster, C., Vereecken, H., 2007. Evaluation of a low-cost soil water content sensor for wireless network applications. J. Hydrol. 344, 32–42. http://dx.doi.org/10.1016/j.jhydrol.2007.06.032.

Boufadel, M.C., 2000. A mechanistic study of nonlinear solute transport in a groundwater-surface water system under steady state and transient hydraulic conditions. Water Resour. Res. 36, 2549–2565.

Boufadel, M.C., Li, H., Suidan, M.T., Venosa, A.D., 2007. Tracer studies in a laboratory beach subjected to waves. J. Environ. Eng. 133, 722–732. http://dx.doi.org/10.1061/(ASCE)0733-9372(2007)133:7(722).

Boufadel, M., Xia, Y., Li, H., 2011. Modeling solute transport and transient seepage in a laboratory beach under tidal influence. Environ. Model. Softw. 26, 899–912. http://dx.doi.org/10.1016/j.envsoft.2011.02.005.
Brovelli, A., Mao, X., Barry, D.A., 2007. Numerical modeling of tidal influence on density-dependent contaminant transport. Water Resour. Res. 43, 1–15. http://dx.doi.org/10.1029/2006WR005173.
Butt, T., Russell, P., Turner, I., 2001. The influence of swash infiltration–exfiltration on beach face sediment transport: onshore or offshore? Coast. Eng. 42, 35–52.
Cartwright, N., Baldock, T.E., Nielsen, P., Jeng, D.-S., Tao, L., 2006. Swash-aquifer interaction in the vicinity of the water table exit point on a sandy beach. J. Geophys. Res. 111. http://dx.doi.org/10.1029/2005JC003149.
Charbonnier, C., Anschutz, P., Poirier, D., Bujan, S., Lecroart, P., 2013. Aerobic respiration in a high-energy sandy beach. Mar. Chem. 155, 10–21. http://dx.doi.org/10.1016/j.
Charette, M.A., Sholkovitz, E.R., 2002. Oxidative precipitation of groundwater-derived ferrous iron in the subterranean estuary of a coastal bay. Geophys. Res. Lett. 29. http://dx.doi.org/10.1029/2001GL014512.
Gallagher, D.L., Dietrich, A.M., Reay, W.G., Hayes, M.C., Simmons, G.M., 1996. Ground water discharge of agricultural pesticides and nutrients to estuarine surface water. Ground Water Monit. Remediat. 16, 118–129.
Hegge, B.J., Masselink, G., 1991. Groundwater-table responses to wave run-up: an experimental study from Western Australia. J. Coast. Res. 7, 623–634.
Horn, D.P., Baldock, T., Baird, A., 1998. Field measurements of swash induced pressure gradients within a sandy beach. In: Proceedings 26th International Conference Coastal Engineering. ASCE, Reston, Virginia, pp. 2812–2825.
Horn, D., Li, L., 2006. Measurement and modelling of gravel beach groundwater response to wave run-up: effects on Beach profile changes. J. Coast. Res. 225, 1241–1249. http://dx.doi.org/10.2112/06A-0006.1.
Kang, H.-Y., Nielsen, P., Hanslow, D.J., 1994. Watertable overheight due to wave runup on a sandy beach. In: Proceedings 24th International Conference Coastal Engineering2. ASCE, Reston, Virginia, pp. 2115–2124.
Kraft, J.C., 1971. The migration of Holocene sedimentary environments in coastal Delaware, North American Continental Shelf. Quaternaria 14, 23–38.
Kroeger, K.D., Charette, M.A., 2008. Nitrogen biogeochemistry of submarine groundwater discharge. Limnol. Oceanogr. 53, 1025–1039.
Li, L., Barry, D.A., Stagnitti, F., Parlange, J.-Y., 1999. Submarine groundwater discharge and associated chemical input to the coastal sea. Water Resour. Res. 35, 3253–3259.
Li, H., Boufadel, M.C., Weaver, J.W., 2008. Tide-induced seawater-groundwater circulation in shallow beach aquifers. J. Hydrol. 352, 211–224.
Longuet-Higgins, M.S., 1983. Wave set-up, percolation and undertow in the surf zone. Proc. R. Soc. Lond. Series A, Math. Phys. Sci. 390, 283–291. http://dx.doi.org/10.1098/rspa.1983.0132.
Loveless, A.M., Oldham, C.E., 2009. Natural attenuation of nitrogen in groundwater discharging through a sandy beach. Biogeochemistry 98, 75–87. http://dx.doi.org/10.1007/s10533-009-9377-x.
Masselink, G., Turner, I.L., 2012. Large-scale laboratory investigation into the effect of varying back-barrier lagoon water levels on gravel beach morphology and swash zone sediment transport. Coast. Eng. 63, 23–38. http://dx.doi.org/10.1016/j.coastaleng.2011.12.007.
Maurmeyer, E.M., 1974. Analysis of Short and Long-term Elements of Coastal Change in a Simple Spit System: Cape Henlopen, Delaware. M.S. Thesis. University of Delaware, Newark, Delaware, p. 150.
McLachlan, A., 1979. Volumes of sea water filtered through Eastern Cape sandy beaches. S. Afr. J. Sci. 75, 75–79.
McLachlan, A., Eliot, I.G., Clarke, D.J., 1985. Water filtration through reflective microtidal beaches and shallow sublittoral sands and its implications for an inshore ecosystem in Western Australia. Estuar. Coast. Shelf Sci. 21, 91–104.
Michael, H.A., Mulligan, A.E., Harvey, C.F., 2005. Seasonal oscillations in water exchange between aquifers and the coastal ocean. Nature 436, 1145–1148.
Naba, B., Boufadel, M.C., Weaver, J., 2002. The role of capillary forces in steady-state and transient seepage flows. Ground Water 40, 407–415.
Nielsen, P., 1990. Tidal dynamics of the water table in beaches. Water Resour. Res. 26, 2127–2134. http://dx.doi.org/10.1029/WR026i009p02127.
Orr, M., Zimmer, M., Jelinski, D.E., Mews, M., 2005. Wrack deposition on different beach types: spatial and temporal variation in the pattern of subsidy. Ecology 86, 1496–1507.
Pollock, L.W., Hummon, W.D., 1971. Cyclic changes in interstitial water content, atmospheric exposure, and temperature in a marine beach. Limnology Oceanogr. 16, 522–535.
Robinson, M.A., Gallagher, D., Reay, W., 1998. Field observations of tidal and seasonal variations in groundwater discharge to tidal estuarine surface water. Ground Water Monit. Remediat. 18, 83–92.
Robinson, C., Gibbes, B., Li, L., 2006. Driving mechanisms for groundwater flow and salt transport in a subterranean estuary. Geophys. Res. Lett. 33. http://dx.doi.org/10.1029/2005GL025247.
Robinson, C., Li, L., Prommer, H., 2007. Tide-induced recirculation across the aquifer-ocean interface. Water Resour. Res. 43. http://dx.doi.org/10.1029/2006WR005679.
Rosenbaum, U., Huisman, J.A., Vrba, J., Vereecken, H., Bogena, H.R., 2011. Correction of temperature and electrical conductivity effects on dielectric permittivity measurements with ECHO sensors. Vadose Zone J. 10, 582.
Santoro, A., 2009. Microbial nitrogen cycling at the saltwater-freshwater interface. Hydrogeol. J. 18, 187–202. http://dx.doi.org/10.1007/s100400090526z.
Santos, I.R., Burnett, W.C., Chanton, J., Mwashote, B., Suryaputra, I.G.N.A., Dittmar, T., 2008. Nutrient biogeochemistry in a Gulf of Mexico subterranean estuary and groundwater-derived fluxes to the coastal ocean. Limnol. Oceanogr. 53, 705–718. http://dx.doi.org/10.4319/lo.2008.53.2.0705.
Short, A.D., 2006. Australian beach systems – nature and distribution. J. Coast. Res. 22, 11–27. http://dx.doi.org/10.2112/05A-0002.1.
Sieyes, N.R., Yamahara, K.M., Layton, B.A., Joyce, E.H., Boehm, A.B., 2008. Submarine discharge of nutrient-enriched fresh groundwater at Stinson Beach, California is enhanced during neap tides. Limnol. Oceanogr. 53, 1434–1445.
Spiteri, C., Slomp, C.P., Charette, M.A., Tuncay, K., Meile, C., 2008. Flow and nutrient dynamics in a subterranean estuary (Waquoit Bay, MA, USA): field data and reactive transport modeling. Geochim. Cosmochim. Acta 72, 3398–3412.
Steenhauer, K., Pokrajac, D., O'Donoghue, T., Kikkert, G.A., 2011. Subsurface processes generated by bore-driven swash on coarse-grained beaches. J. Geophys. Res. 116. http://dx.doi.org/10.1029/2010JC006789.
Steenhauer, K., Pokrajac, D., O'Donoghue, T., 2012. Numerical model of swash motion and air entrapment within coarse-grained beaches. Coast. Eng. 64, 113–126. http://dx.doi.org/10.1016/j.coastaleng.2012.01.004.
Turner, I.L., 1993a. The total water content of sandy beaches. J. Coast. Res. (Special Issue No. 15), 11–26.
Turner, I.L., 1993b. Water table outcropping on macro-tidal beaches: a simulation model. Mar. Geol. 115, 227–238.
Turner, I.L., Acworth, R.I., 2004. Field measurements of beachface salinity structure using cross-borehole resistivity imaging. J. Coast. Res. 20, 753–760.
Turner, I.L., Masselink, G., 2012. Coastal gravel barrier hydrology – observations from a prototype-scale laboratory experiment (BARDEX). Coast. Eng. 63, 13–22. http://dx.doi.org/10.1016/j.coastaleng.2011.12.008.
Turner, I.L., Masselink, G., 1998. Swash infiltration–exfiltration and sediment transport. J. Geophys. Res. 103, 30813–30824.
Turner, I.L., Nielsen, P., 1997. Rapid water table fluctuations within the beach face: implications for swash zone sediment mobility? Coast. Eng. 32, 45–59 http://dx.doi.org/10.1016/S0378-3839(97)00015-X.
Ullman, W.J., Chang, B., Miller, D.C., Madsen, J.A., 2003. Groundwater mixing, nutrient diagenesis, and discharges across a sandy beachface, Cape Henlopen, Delaware (USA). Estuar. Coast. Shelf Sci. 57, 539–552.
Vandenbohede, A., Lebbe, L., 2005. Occurrence of salt water above fresh water in dynamic equilibrium in a coastal groundwater flow system near De Panne, Belgium. Hydrogeol. J. 14, 462–472. http://dx.doi.org/10.1007/s10040-005-0446-5.
Van Genuchten, M.T., 1980. Closed-form equation for predicting the hydraulic conductivity of unsaturated soils. Soil. Sci. Soc. Am. J. 44, 892–898.
Vukovic, M., Soro, A., 1992. Determination of Hydraulic Conductivity of Porous Media from Grain-Size Composition. Water Resources Publications, Littleton, CO, p. 83.
Waddell, E., 1976. Swash-groundwater-beach profile interactions. In: Davis, R.A., Etherington, R.L. (Eds.), Beach and Nearshore Sedimentation. Society of Economic and Paleontological Mineralogists Special Publication 24, Tulsa, OK, pp. 115–125.